Boron nitride for enhanced oxidative dehydrogenation of ethylbenzene

Rui Han[a,b], Jiangyong Diao[c], Sonu Kumar[d], Andrey Lyalin[d,e], Tetsuya Taketsugu[d,f], Gilberto Casillas[g], Christopher Richardson[h], Feng Liu[a,b], Chang Won Yoon[i], Hongyang Liu[c,*], Xudong Sun[a,*], Zhenguo Huang[b,*]

[a] *Key Laboratory for Anisotropy and Texture of Materials (Ministry of Education), Northeastern University, Shenyang 110819, China*
[b] *School of Civil & Environmental Engineering, University of Technology Sydney, Ultimo, New South Wales 2007, Australia*
[c] *Shenyang National Laboratory for Materials Science, Institute of Metal Research, Chinese Academy of Sciences, Shenyang, Liaoning 110016, China*
[d] *Institute for Chemical Reaction Design and Discovery (WPI-ICReDD), Hokkaido University, Sapporo 001-0021, Japan*
[e] *Center for Green Research on Energy and Environmental Materials, National Institute for Materials Science (NIMS), Tsukuba 305-0044, Japan*
[f] *Department of Chemistry, Faculty of Science, Hokkaido University, Sapporo 060-0810, Japan*
[g] *Electron Microscopy Centre, University of Wollongong, New South Wales 2500, Australia*
[h] *Molecular Horizons and School of Chemistry & Molecular Bioscience, Faculty of Science, Medicine & Health, University of Wollongong, New South Wales 2522, Australia*
[i] *Center for Hydrogen and Fuel Cell Research, Korea Institute of Science and Technology, Seoul 02792, Republic of Korea.*

[*]Corresponding authors.
E-mail addresses: zhenguo.huang@uts.edu.au (Z. Huang);
xdsun@neu.edu.cn (X. Sun);
liuhy@imr.ac.cn (H. Liu)

ABSTRACT

It is demonstrated experimentally and confirmed theoretically that highly defective boron nitride showed outstanding performance for oxidative dehydrogenation of ethylbenzene. The catalyst is derived from carbon-doped hexagonal boron nitride nanosheets synthesized via a two-step reaction when participating the oxidative dehydrogenation reaction. The first step yields a polymeric precursor with the atomic positions of B, C, N relatively constrained, which is conducive for the formation of carbon atomic clusters uniformly dispersed throughout the BN framework. During the oxidative dehydrogenation of ethylbenzene to styrene, the nanoscale carbon clusters are removed and highly defective boron nitride (D-BN) is obtained, exposing boron-rich zigzag edges of BN that act as the catalytic sites. The catalytic performance of D-BN is therefore remarkably better than un-doped h-BN. Our results indicate that dispersed C-doping in h-BN is highly effective in terms of defect formation and resultant enhanced activity in oxidative dehydrogenation reactions.

Keywords: Boron nitride; dehydrogenation; ethylbenzene; carbon-doping; heterogeneous catalysis

1. Introduction

The production of styrene is a very important industrial process. The conventional direct dehydrogenation of ethylbenzene in the presence of steam over iron oxide suffers from low conversion due to thermodynamic limitations [1,2]. Oxidative dehydrogenation (ODH) is an alternative to direct dehydrogenation of hydrocarbons to produce high-value-added alkenes in modern chemical industry. The ODH process features a) an overall exothermic reaction, b) the presence of oxygen in the reaction that

prevents formation of coke, and c) high alkane conversions [3-6]. Carbon materials such as activated carbon, carbon nanotubes, graphene, etc. have been studied extensively as oxidation catalysts due to their rich surface chemistry that is achieved through functionalization [7-14]. However, oxidative dehydrogenation using carbon-based catalysts still suffer from poor oxidation resistance and coke formation which cause catalyst deactivation [15].

Recently, hexagonal boron nitride based materials have been discovered as novel ODH catalysts. In Hermans' pioneering study, hexagonal boron nitride and BN nanotubes demonstrated unique ODH performance with 79% propene selectivity at 14% propane conversion, where oxygen-terminated armchair BN edges were suggested as the catalytic active sites [16]. Another study found edge hydroxylated h-BN effective in ODH of propane [17].

Carbon-doped BN (C-BN) has also shown interesting performance as a catalyst for ODH of ethylbenzene, and it is believed that carbon plays a key role in this process [5]. One of the most common routes to synthesize C-BN is through one-step pyrolysis of boric acid and urea or melamine, with glucose as the source of carbon [18-22]. This method can create C-BN with very large surface areas, but it often leads to materials featuring patches of C clusters with large lateral sizes. This is because it is more thermodynamically favorable to form large graphene and BN domains, rather than small C atomic clusters uniformly distributed in BN framework [23,24]. Intuitively, these large C clusters would behave more like carbon-only materials, and this is likely to reduce the stability of C-BN catalysts.

Herein, we report a novel two-step reaction route that produces carbon-doped hexagonal boron nitride nanosheets (h-BN) with a highly uniform distribution of C atomic clusters. When these materials are used in the ODH reaction of ethylbenzene,

the C clusters are removed, forming highly defective BN (D-BN) that becomes an outstanding catalyst, with 89% styrene selectivity at 52% ethylbenzene conversion. The process features a short induction period with no sign of performance decay after 30 h on stream. The enhancement, in comparison with undoped h-BN, is believed to be associated with a greater number of active BN edge sites created by the removal of small C clusters during ODH process.

2. Experimental

2.1. Synthesis of h-BN nanosheets

For a typical experiment, a mixture of ammonia borane (200 mg) (Sigma-Aldrich) and ethylenediamine (0.4 mL) (Sigma-Aldrich) in an autoclave under argon atmosphere was placed in an oven at 120 °C for 24 hours. After that, the off-white solid product was collected and mixed with NH_4Cl (2 g) (Sigma-Aldrich). The mixture was then transferred to a horizontal tube furnace and heated up to 1000 °C for 3 hours under an atmosphere of ammonia. The resulting yellow powders are denoted h-BN.

2.2. Characterization methods

X-ray powder diffraction (XRD) patterns were acquired on a GBC MMA with Cu Kα radiation at a step size of 2θ = 0.02° and a speed of 2° min^{-1}. Attenuated total reflection Fourier transform infrared (ATR-FTIR) spectroscopy study was conducted on a Shimadzu FTIR Prestige-21. Raman spectra were collected on a Horiba Raman JY HR-800 spectrometer using a 632.81 nm laser source. Scanning electron microscopy (SEM) was performed on the JEOL-JSM-7500. A JEOL ARM200F was utilized to conduct transmission electron microscopy (TEM) and scanning transmission electron microscopy (STEM) study. X-Ray photoelectron spectra (XPS) were collected on an

ESCALAB250Xi with a mono-chromated Al Kα source. Thermogravimetric analysis (TGA) was performed on Netzsch STA 449 F5 Jupiter thermal analyzer, which is coupled with gas chromatography and mass spectrometer (GC-MS, Agilent 7890/5977). Surface area analysis was performed on a Quantachrome Autosorb MP analyzer using high purity N_2 gas (99.995%).

2.3. Catalytic tests

The ODH catalytic test was carried out at 550 °C under atmospheric pressure. For a typical experiment, 50 mg of h-BN catalyst was loaded to a fixed-bed quartz reactor and fixed between two quartz wool plugs. The system was kept for 10 min under helium after it reached 550 °C. The reactant consisted of 2.8% ethylbenzene and 5.6% O_2 with helium as balance carrier gas. The reactant with a total flow rate of 10 ml min^{-1} was then fed to the reactor from a saturator kept at 39.8 °C. A on-line gas chromatograph used to analyze the reactants was equipped with a HP-5 capillary column connected to a flame ionization detector (FID) for hydrocarbons and a CarboPlot capillary coupled to a thermal conductivity detector (TCD) for permanent gases. The ethylbenzene conversion (X_{EB}) and styrene selectivity (S_{ST}) were calculated according to the following equations:

$$X_{EB} = 1\text{-}FC_{EB,\,outlet}/\,F_0C_{EB,\,inlet}$$

$$S_{ST} = C_{ST,\,outlet}/\,(C_{ST,\,outlet} + C_{BZ,\,outlet} + C_{TOL,\,outlet})$$

$$Y_{ST} = X_{EB} * S_{ST}$$

F and F_0 are the flow rates of the outlet and inlet. C_{EB}, C_{ST}, C_{BZ}, and C_{TOL} denote the concentrations of ethylbenzene, styrene, benzene, and toluene, respectively.

3. Results and discussion

3.1. Structure of the h-BN catalyst

The h-BN was prepared via a two-step synthesis (Scheme 1). Firstly, reacting ammonia borane with ethylenediamine leads to a polymeric precursor where the C, B, and N atomic positions are fixed relatively to each other, i.e., avoiding the agglomeration of C atoms. Secondly, the polymeric precursor is annealed under an atmosphere of ammonia at an elevated temperature to obtain h-BN with small C domains uniformly distributed in the BN matrix. The as-prepared h-BN is largely amorphous but does exhibit a graphitic layered structure as evidenced by two broad peaks in the XRD pattern (Fig. 1a). The peaks at 24.5° and 43° correspond to the (002) and (100) reflections, respectively. Based upon Bragg's law, the *d* spacing along [002] is 0.35 nm, slightly larger than this in highly crystalline hexagonal boron nitride [17]. FTIR spectrum (Fig. 1b) reveals two bands at 1390 cm^{-1} and 800 cm^{-1}, which are attributed to in-plane stretching and out-of-plane bending modes of hexagonal boron nitride [25]. The B-C vibration can be found at approximately 1110 cm^{-1} [26]. The typical C-N and C=N vibrations in the range from 1100 cm^{-1} to 1600 cm^{-1} are not distinguishable in the spectrum, because these vibrations are relatively weak and can be overwhelmed by the high intensity B-N stretching band [27]. The Raman spectrum of h-BN is featureless due to the disruption of in-plane symmetry brought by incorporation of C atoms in the BN plane. By virtue of the spectrum not displaying the characteristic bands for graphite or hexagonal boron nitride, this indicates the dopant C atoms are well dispersed in the BN framework without forming large carbon agglomerates [20]. The atomic ratio of C in the h-BN revealed by XPS is only 3.44%, much lower than what is typically found in the C-BN by direct pyrolysis (Table S1). Another sample (denoted h-BN*) with the same amount of ammonia borane (200 mg)

but half the amount of ethylenediamine (0.2 mL) in the precursor mix was synthesized under the same experimental parameters, aiming to produce a sample with lower C content. But the C content is largely the same according to XPS (Table S1). This is in agreement with literature report that NH_3 removes large amounts of carbon at high temperature annealing [28].

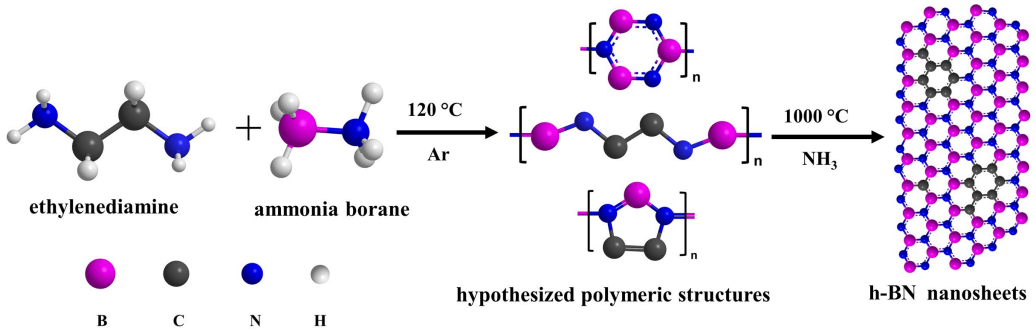

Scheme 1. The two-step synthesis of h-BN nanosheets. Hydrogen atoms are omitted in the hypothesized polymeric structures.

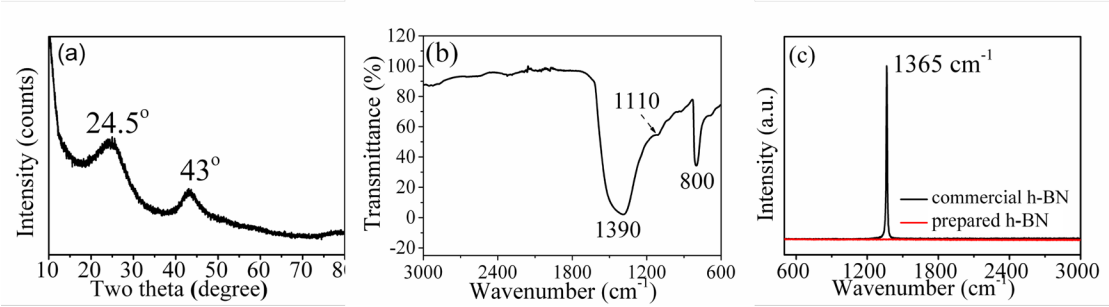

Fig. 1. (a) XRD pattern, (b) FTIR spectrum, and (c) Raman spectrum of h-BN.

The porous structure of h-BN was characterized by surface area analysis (Fig. S2). The N_2 adsorption-desorption isotherms at 77 K present a type-II curve with H4 hysteresis. The pore size distribution shows a dominant peak at around 1 nm, indicating the formation of large proportion of micropores. The surface area obtained from BET calculations is 158 $m^2 g^{-1}$. While this is lower compared to some C-BN synthesized via

one-step pyrolysis [18,29], a modest surface area would be less likely to hinder desorption of styrene [7,8,30].

The prepared h-BN adopts a planar structure with lateral particle sizes ranging from several hundreds of nanometers to microns (Fig. 2a, b). High resolution bright field TEM analysis reveals that the nanosheets are crumpled with few-atomic-layer thickness (Fig. 2c). The interlayer distance was measured to be 0.35 nm, 0.02 nm larger than that of (002) spacing of hexagonal boron nitride crystal, which agrees with the XRD results. The slightly enlarged interlayer distance is likely due to the delamination effect brought about by the incorporation of C atoms in the BN's framework, as suggested in the Raman spectrum [18]. In the high angle angular dark field STEM (HAADF-STEM) image, B, C, N atoms can be differentiated according to their Z contrast [31,32]. In a relatively thin region, we managed to detect a possible C doping site and a B vacancy in the Fast Fourier Transform (FFT) filtered HAADF-STEM image (Fig. S3). However, due to relatively low S/N ratio and sharpness caused by curling of the nanosheets and drift of the microscope at high resolution, the atomic number may not be accurately reflected by HAADF intensity of the atoms.

The chemical composition was examined by electron energy loss spectroscopy (EELS), which is much more sensitive in detecting light elements and has much higher spatial resolution compared with energy-dispersive X-ray spectroscopy (EDS) [33,34]. The EELS spectrum shows characteristic B and N K-edge features, starting from 188.2 eV and 398.6 eV, respectively. The presence of 1s-π* to 1s-σ* anti-bonding orbitals in both B and N peaks indicates the formation of sp^2 hybridization in BN regions [35]. A set of peaks with modest intensity starting from 282.5 eV are observed, and these are attributed to the C K-edge ionization energies. To investigate the distribution of C within the materials, EELS mapping was performed with a probe size of 0.75 nm ×

0.75 nm (Fig. 2f). In the C K-edge (282.5-312.5 eV) map, we can observe that C atoms are distributed in small atomic clusters all over the h-BN nanosheets. The differences in the intensity may be partly due to folding of the sheets and differences in thickness. Therefore, it is reasonable to say that C atoms are uniformly doped at atomic level in the BN framework.

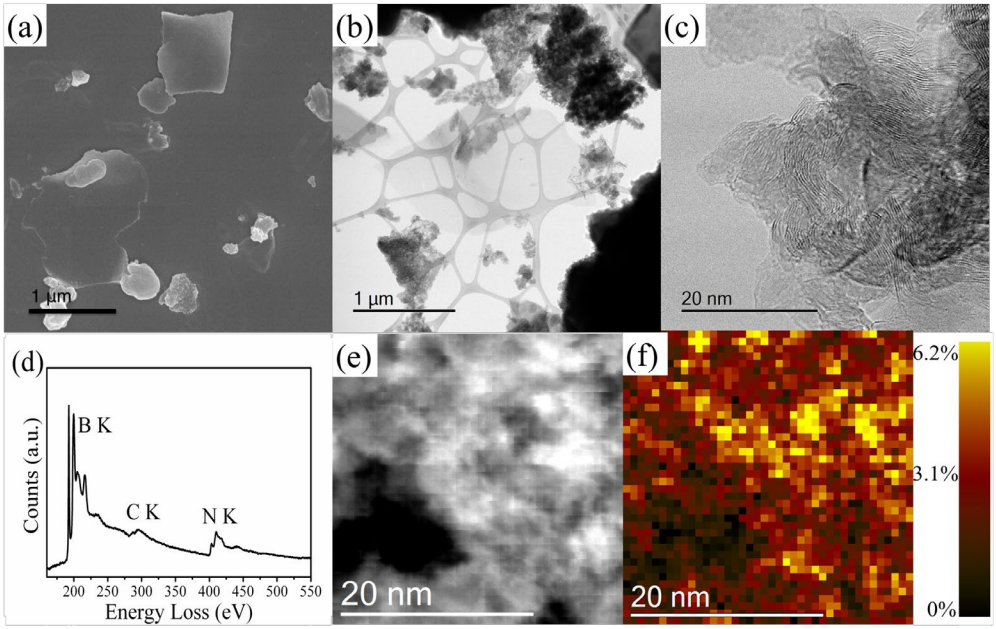

Fig. 2. Electron microscopic characterization of h-BN: (a) SEM image; (b) Bright field STEM image; (c) High resolution bright field STEM image; (d) EELS spectrum; (e) and (f) EELS mapping of carbon with a spot size of 0.75 nm × 0.75 nm.

Previous studies have found that C atoms tend to fuse together forming large graphene domains in C-doped BN matrix, and this is attributed to favorable thermodynamics [23,24]. In this work, the relative atomic positions of B, C, N atoms are pre-locked in a relatively thermally stable polymeric precursor (Scheme 1), which is believed to prevent the fusion of C atoms during heat treatment. FTIR spectroscopy was employed to investigate the chemical bonds in the polymeric precursor obtained by reacting ammonia borane with ethylenediamine (ABE) in an autoclave at 120 °C

during the first step. A thermal decomposition product of ammonia borane (AB) obtained under the same reaction conditions was studied as a reference. For reference AB, there are two IR bands situated between 1100 cm^{-1} and 1200 cm^{-1} attributed to BH_2 deformation [36], which are weaker in the precursor of ABE (Fig. 3a). In addition, N–H stretch around 3285 cm^{-1} is nearly invisible and a weak C–H stretch around 2885 cm^{-1} is observed in the ABE, further indicating that ammonia borane reacts with ethylenediamine during the first step. A shoulder band at 1270 cm^{-1} was seen in the ABE precursor which corresponds to C–N stretching vibration. Noticeably, this C–N band is located at a wavenumber close to that of aromatic C–N stretching band, which is quite different from the aliphatic amine C–N stretch at ~1040 cm^{-1} that can be found in ethylenediamine [37-39]. The appearance of an aromatic C–N stretch suggests the formation of B, N and C heterocycles. Moreover, a red shift of 30 cm^{-1} was found for the B–N in-plane stretching in the ABE precursor in comparison with AB reference, likely caused by the formation of B–N–C. The IR spectra also hint that the first step treatment has removed most of hydrogen atoms, since B–H, N–H, and C–H stretches are weak or invisible. The reaction between ammonia borane and ethylenediamine is possibly driven by $N{-}H^{\delta+}\cdots H^{\delta-}{-}B$ dihydrogen interactions [40], where negatively charged H is from $NH_3\mathit{BH}_3$ and positively charged H is from $\mathit{NH}_2CH_2CH_2\mathit{NH}_2$. The C atoms are therefore confined in the hydrogen-lean polymeric precursor that features >B–N–C–C–N< units (Scheme 1). During high temperature treatment in the second step, this precursor will unlikely experience much dehydrogenation and a large-scale re-arrangement of B, C, N atoms is prevented [41]. This is believed to be instrumental in the formation of uniform dispersion of C dopants in the final product (Fig. 2f).

To assess the thermal stability of h-BN, thermal gravimetric analysis was

conducted in dry air up to 1000 °C. As shown in Fig. 3b, h-BN shows good thermal stability with less than 10% weight loss up to 850 °C, with oxidation at higher temperatures causing rapid weight gain. The evolution of CO_2, resulting from oxidation of C dopants by O_2 in the gas stream, is observed in the extracted ion chromatograph (EIC) by the increased emissions at 200 °C and 450 °C. It is reasonable to predict that under the conditions of ODH (550 °C in the presence of O_2), C atoms are removed from the h-BN framework leading to the formation of defective hexagonal boron nitride (D-BN) with highly reactive BN edges. Since the chemical structure changes when h-BN evolves into D-BN during the ODH reaction, it is necessary to investigate the structural information of D-BN. h-BN was calcined in air at 550 °C to mimic D-BN and the product after calcination is denoted D-BN*. D-BN* maintains the nanosheet morphology (**Fig.** S6) and its Raman spectrum remains featureless due to the highly defective structure. FTIR spectra (Fig. 4) reveal that carbon is mostly removed from the BN framework as the B-C band located at ~1110 cm^{-1} weakens in D-BN*. The appearance of -OH band at ~3200 cm^{-1} and B-O band at ~1200 cm^{-1} indicates the formation of B-OH species when h-BN is heated at 550 °C under air [42,43].

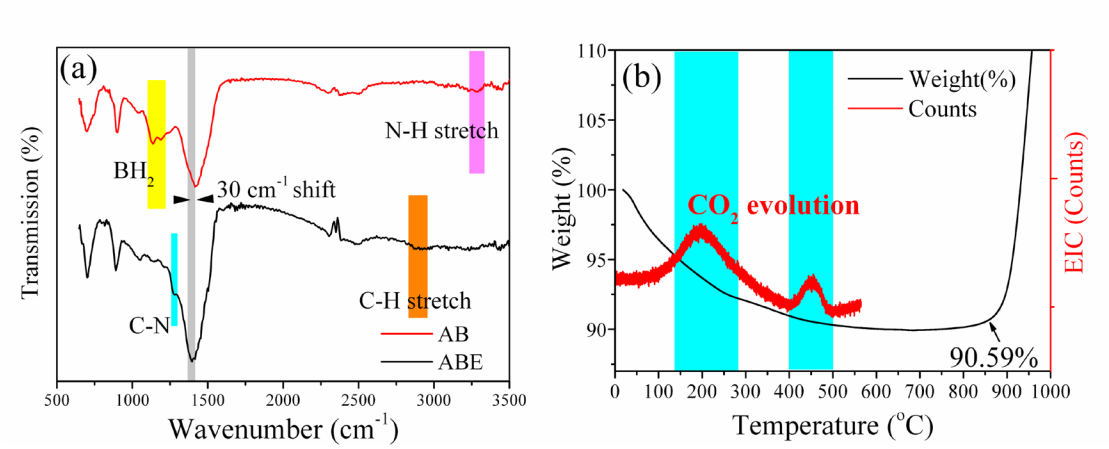

Fig. 3. (a) FTIR spectra of polymeric precursors obtained from the first step reaction. (b) TG curve for h-BN (black curve) up to 1000 °C and extracted ion chromatographs (EIC) (red curve) for m/z = 44 up to 560 °C under air.

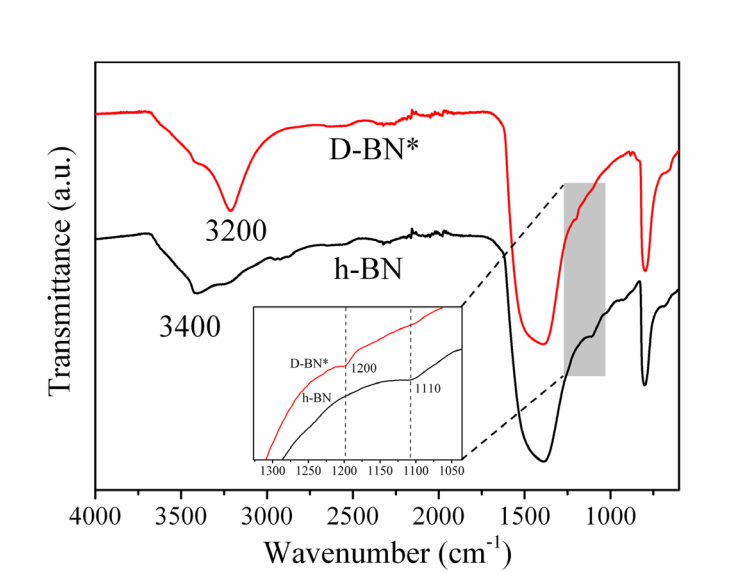

Fig. 4. FTIR spectra of D-BN* and h-BN indicate the formation of B-OH species when h-BN is heated at 550 °C under air.

3.2. Catalytic Performance of the D-BN catalyst

The catalytic performance of the h-BN derived D-BN on ODH of ethylbenzene to styrene was evaluated at 550 °C and is represented graphically in Fig. 5. After a 3 h induction period, ethylbenzene conversion and styrene selectivity both plateaued at 52% and 89%, respectively (Fig. 5). For comparison, the catalytic ODH behavior of commercial h-BN and an un-doped h-BN reference sample obtained by direct pyrolysis of ammonia borane (denoted undoped h-BN) was also investigated (Fig. 5b & Fig. S4). The carbon balance is nearly 100%. Commercial h-BN and undoped h-BN both showed obvious deactivation after 5 h with ethylbenzene conversion only reaching 21% and 9% at the 25 h mark, respectively (Fig. S4). In contrast, reactions catalyzed by D-BN quickly stabilized at above 50% conversion after 5 h with no sign of diminishment in performance out to 30 hours, indicating high stability of the catalytic sites. Table S3. compares the catalytic performance of different catalysts for ODH conversion of ethylbenzene. It can be seen that the D-BN catalyst has outstanding catalytic

performance with a high ethylbenzene conversion and styrene formation rate in comparison with other reported catalysts.

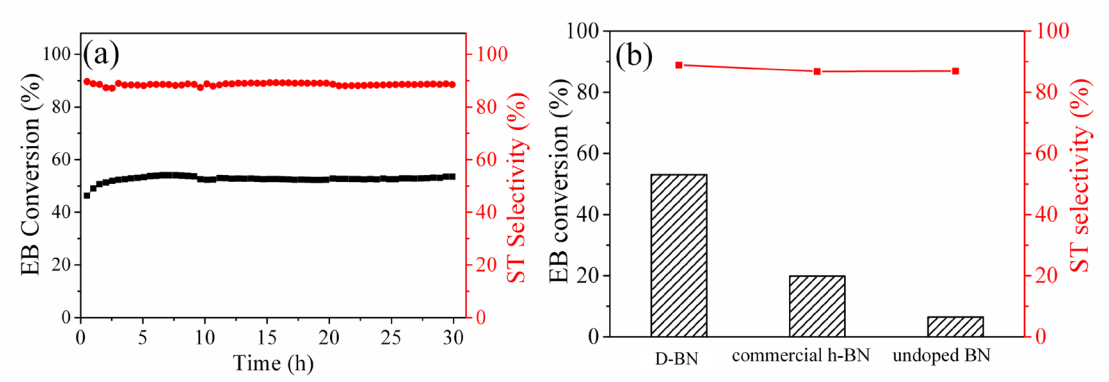

Fig. 5. (a) The performance of D-BN in ODH converting ethylbenzene (EB) into styrene (ST). Reaction condition: 50 mg catalyst, 2.8% ethylbenzene with He balance, O_2/ethylbenzene = 2, total flow rate = 10 mL min^{-1}, T = 550 °C. (b) ODH performance of h-BN, commercial h-BN and undoped h-BN at 25 h.

XPS was conducted to investigate the change in chemical compositions before and after the ODH reaction to provide insights on the reaction mechanism. The survey spectra and peak table are provided in the Supporting Information (Fig. S5, Table S2) and high-resolution spectra of C and O elements are shown in Fig. 6. It is notable that the N/B ratio decreases sharply from 0.916 to 0.745 after the ODH reaction, indicating the sample becomes B-rich and highly defective after ODH. In addition, O content increases significantly and the peak position mostly correlates to B–O, which is more stable than N–O [44]. This is interpreted as the creation of D-BN with oxygen functionalized boron species during the induction which facilitate the rapid increase of the catalytic activity [43, 45]. During the ODH reaction, the freshly formed B–O(H) groups by the removal of C dopants and N atoms give rise to the high and stable conversion of ethylbenzene, and is in contrast to the observed degradation in

performance by the undoped h-BN and commercial h-BN samples.

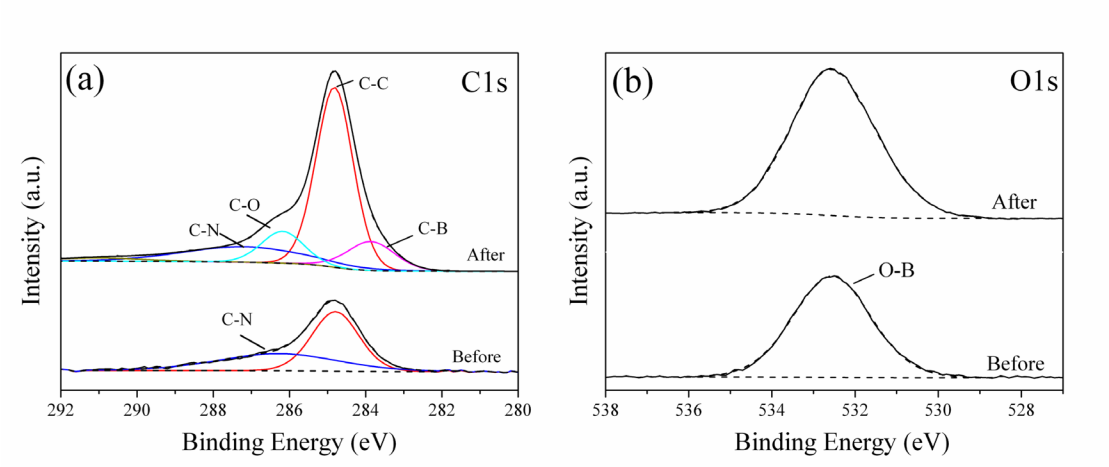

Fig. 6. XPS spectra of C and O before and after the ODH reaction. Note that the intensities in the spectra have been scaled for easy comparison.

Despite deposition of carbon being observed on the D-BN catalyst (Table S2 & Fig. 6b), it does not contribute significantly to the catalytic performance for the following reasons. Firstly, the deposited carbon exists mainly in the form of adventitious carbon resulted from adsorption of reactant, as can be seen in the C XPS peak (Fig. 6a). Secondly, it is widely accepted that surface ketonic carbonyl groups (C=O), formed *in situ* when carbon reacts with molecular oxygen, are the active sites of carbon catalysts for ODH [46, 47]. However, there is no component correlating to C=O groups (~289 eV) in the C peaks of the catalyst after the ODH reaction. This indicates that the deposited carbon on our D-BN catalyst does not react with molecular oxygen to form active species. This is further proven by the O XPS peaks in Fig. 5b where the peak position and shape remain unchanged and only B–O (532.5 eV) is observed. The C=O groups typically situated at 531 eV is missing in the O XPS peak after the ODH reaction. Therefore, these results clearly illustrate that the catalytic activity is mainly provided by the D-BN catalyst rather than the carbon deposit formed during the ODH.

The styrene selectivity and ethylbenzene conversion of our catalyst are comparable to but more stable than those of carbon-doped BN catalyst with a surface area of 1450 $m^2 g^{-1}$ and carbon content over 12% [5]. The reported carbon-doped BN catalyst shows obvious performance decay after 20 h, which is absent in the D-BN in this work. It is interesting to note that dramatic differences in the specific surface area and carbon content do not result in differences in catalytic activity. It can be then inferred that the catalytic activity does not stem from the vast majority –B–N– sites in the BN plane as the change in the surface area exerts little impact on the catalytic behavior. Furthermore, the higher carbon content in the reported sample do not lead to better and stable performance compared with our sample, indicating that larger patches of graphene domains in BN are not active in creating catalytic centers. These observations lead us to believe that the uniformly dispersed nanoscale carbon clusters, when gradually removed during ODH reaction, can create D-BN with more reactive sites, which is crucial to the high and stable ethylbenzene conversion.

3.3. Theoretical studies

In order to get a clearer understanding of the catalytic process, theoretical studies were carried out. Density functional theory (DFT) calculations were performed using the Quantum Espresso package [48,49] along with the projector augmented wave (PAW) based pseudopotentials approach [50,51]. The generalized gradient-corrected approximation with the parametrization of Perdew−Burke−Ernzerhof (PBE) [52] for the exchange-correlation functional was used. Further computational details and theoretical methods are given in the Supporting Information. Previously two structural models have been suggested for possible active sites of ODH on boron nitride catalysts. Grant et al. [16] proposed that the O-terminated armchair BN edges are responsible for

selective ODH of propane to propene, while in Ref. [17] it was suggested that the edge-hydroxylated sites at the O-terminated zigzag edges of boron nitride >B–O–H H–O–B< serve as the catalytically active centers. It is important to note that O-terminated boron rich zigzag edges are stable terminations in BN, leading to stabilization of the small triangular defects in h-BN sheets, as was shown theoretically in Ref. [53]. In the present work we have not observed a solid evidence of the edge hydroxylation, therefore based upon the XPS results, we propose a structural model with the >B–O–O–B< active site at the O–terminated B-rich zigzag edge of BN nanoribbon with a width ~ 15 Å passivated from the opposite site by H atoms, as shown in Fig. S1. The large width of the nanoribbon minimizes the size effects on adsorption energies of reaction intermediates. This model cannot of course represent the whole variety of the possible active sites formed in D-BN catalyst; however, it mimics the important features of the catalyst structure observed experimentally, namely the B-rich contents and presence of the B–O bonds as well as it is fully consistent with the theoretical predictions on the high stability of the O-terminated zigzag edge defects in BN. Note, that hydrogenation of the >B–O–O–B< active site proposed in the present work would immediately lead us to the model suggested in Ref. [17].

Fig. 7a shows the free energy profile, ΔG, calculated along the reaction pathway for oxidative dehydrogenation of ethylbenzene to styrene at the >B–O–O–B< active site of the O-terminated zigzag edge of BN. The reaction is a two-step process with the first H transfer from the $–CH_2–$ group of ethylbenzene (C_8H_{10}) resulting in formation of the stable intermediates H^* and $C_8H_9^*$ at the edge of BN nanoribbon (herein adsorbed species are marked by asterisk), followed by C–H bond cleavage from the methyl group.

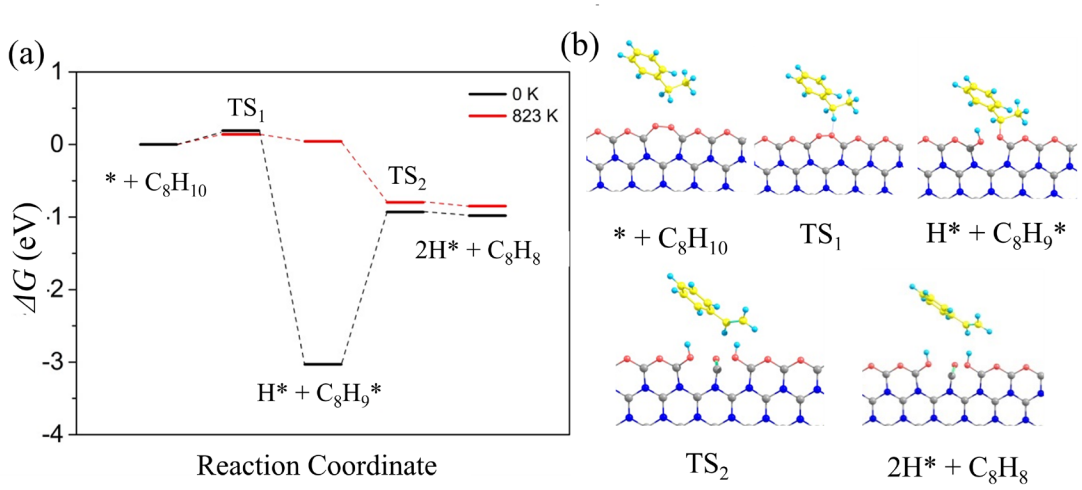

Fig. 7. (a) Change in free energy, ΔG, for conversion of ethylbenzene to styrene calculated at T = 0 K (black) and T = 823 K corresponding to the experimental conditions (red); (b) Optimized atomic structures of intermediates and transition states for the first (TS1) and second (TS2) H transfers along the ODH reaction catalyzed by the >B–O–O–B< active site at the O–terminated B-rich zigzag edge of a BN nanoribbon. C: yellow; H: turquoise; O: red; B: grey; N: blue.

Our calculations show that the first H transfer from the $–CH_2–$ group of C_8H_{10} requires overcoming transition state TS_1 with a barrier height of 0.19 eV at T = 0 K. Formation of strongly associated H^* and $C_8H_9^*$ intermediates is an exothermic process with the ΔG = –2.98 eV in respect to the non-interacting free C_8H_{10} molecule and the BN catalyst. The $C_8H_9^*$ intermediate approaches the edge with formation of the O–C bond which is accompanied by the O–O bond breaking at the >B–O–O–B< site. The corresponding geometry structures are shown in Fig. 7b. At T = 0 K the second H transfer from the $–CH_3$ group of $C_8H_9^*$ with the formation of free styrene product and $2H^*$ species is energetically unfavorable (Fig. 7a). However, increase in temperature destabilizes the bounded $C_8H_9^*$ intermediate in respect to the free final product C_8H_8 leading to the energetically favorable C-H bond cleavage from the methyl group at T >

550 K. Calculations at temperature T = 823 K indicate the barrier for the first H transfer decreases slightly up to 0.14 eV due to the small differences in entropies of the initial and TS_1 configurations, while the second C–H bond cleavage is barrierless. Here an assumption was used that molecular structures in TS_1 and TS_2 are weakly bounded and can be considered as pseudo-free. This assumption results in increase of the entropic contribution to the free energies of the free and pseudo-free species with increasing temperature, because the main contribution to the total entropy arises from the translational degrees of freedom. On the other hand, in the case of the strongly bounded intermediate the translational degrees of freedom are frozen and free energy does not change considerably. Therefore, a strong destabilization of the bounded intermediate in respect to the free molecular species occurs. One should also note that further increase in temperature above 823 K results in destabilization of the $C_8H_9^*$ intermediate in respect to the initial state and further decrease in the reaction rate. Overall, our DFT calculations demonstrate that at T = 823 K oxidative dehydrogenation of ethylbenzene to styrene at the >B–O–O–B< active site of the O-terminated zigzag edge of BN is a highly favorable process with a very small barrier for the first H transfer.

4. Conclusions

In conclusion, we have prepared highly effective h-BN as an ODH catalyst via a novel two-step synthesis, with the first step pre-locking C atoms in the h-BN framework. The catalyst exhibits outstanding catalytic activity in ODH reactions (89% styrene selectivity at 52% ethylbenzene conversion over 30 h). HRTEM and EELS studies confirm that C dopants are uniformly dispersed at the atomic scale in the BN matrix, which is found to be crucial in creating highly defective boron nitride with more active sites during the ODH process. DFT calculations suggest that ODH of ethylbenzene to

styrene at >B–O–O–B< sites is an energetically favorable process at moderately elevated temperatures. This study provides a new insight into the construction of functional BN catalysts in terms of controlling the positions of dopants. More research efforts should be made towards precision doping where the chemical environment of the dopants is defined, which may lead to further improved catalytic performance.

Acknowledgments

Z.H. acknowledges support under the Australian Research Council's Discovery Projects funding scheme (project number DP170101773), and support from Alexander von Humboldt Foundation. A.L. thanks for financial support from the program of the Ministry of Education, Culture, Sports, Science, and Technology (MEXT, Japan) "Priority Issue on Post-K computer" (Development of new fundamental technologies for high-efficiency energy creation, conversion/storage and use). Institute for Chemical Reaction Design and Discovery (ICReDD) was established by World Premier International Research Initiative (WPI), MEXT, Japan. H. L. acknowledges support from the Ministry of Science and Technology (2016YFA0204100), the National Natural Science Foundation of China (21961160722, 91845201, 21573254) and the Liaoning Revitalization Talents Program XLYC1907055.

References

[1] E.H. Lee, Catal. Rev. 8 (1974) 285-305.
[2] L. Shi, G.-M. Deng, W.-C. Li, S. Miao, Q.-N. Wang, W.-P. Zhang, A.-H. Lu, Angew. Chem. Int. Ed. 54 (2015) 13994-13998.
[3] F. Cavani, N. Ballarini, A. Cericola, Catal. Today 127 (2007) 113-131.
[4] C.A. Gärtner, A.C. van Veen, J.A. Lercher, ChemCatChem 5 (2013) 3196-3217.
[5] F. Guo, P. Yang, Z. Pan, X.-N. Cao, Z. Xie, X. Wang, Angew. Chem. Int. Ed. 56 (2017) 8231-8235.
[6] F. Cavani, F. Trifirò, Appl. Catal., A 133 (1995) 219-239.
[7] N. Keller, N.I. Maksimova, V.V. Roddatis, M. Schur, G. Mestl, Y.V. Butenko, V.L. Kuznetsov, R. Schlögl, Angew. Chem. Int. Ed. 41 (2002) 1885-1888.
[8] M.F.R. Pereira, J.J.M. Órfão, J.L. Figueiredo, Appl. Catal., A 184 (1999) 153-160.
[9] J. Zhang, X. Liu, R. Blume, A. Zhang, R. Schlögl, D.S. Su, Science 322 (2008) 73-77.
[10] J. Zhang, D. Su, A. Zhang, D. Wang, R. Schlögl, C. Hébert, Angew. Chem. Int. Ed. 46 (2007) 7319-7323.
[11] X. Liu, B. Frank, W. Zhang, T.P. Cotter, R. Schlögl, D.S. Su, Angew. Chem. Int. Ed. 50 (2011) 3318-3322.
[12] B. Frank, J. Zhang, R. Blume, R. Schlögl, D.S. Su, Angew. Chem. Int. Ed. 48 (2009) 6913-6917.
[13] D.R. Dreyer, H.-P. Jia, C.W. Bielawski, Angew. Chem. Int. Ed. 49 (2010) 6813-6816.
[14] X.-H. Li, M. Antonietti, Angew. Chem. Int. Ed. 52 (2013) 4572-4576.
[15] G.R. Meima, P.G. Menon, Appl. Catal., A 212 (2001) 239-245.
[16] J.T. Grant, C.A. Carrero, F. Goeltl, J. Venegas, P. Mueller, S.P. Burt, S.E. Specht, W.P. McDermott, A. Chieregato, I. Hermans, Science 354 (2016) 1570-1573.
[17] L. Shi, D. Wang, W. Song, D. Shao, W.-P. Zhang, A.-H. Lu, ChemCatChem 9 (2017) 1788-1793.
[18] S. Chen, P. Li, S. Xu, X. Pan, Q. Fu, X. Bao, J. Mater. Chem. A 6 (2018) 1832-1839.
[19] M. Chhetri, S. Maitra, H. Chakraborty, U.V. Waghmare, C.N.R. Rao, Energy & Environ. Sci. 9 (2016) 95-101.
[20] C. Huang, C. Chen, M. Zhang, L. Lin, X. Ye, S. Lin, M. Antonietti, Nature Commun. 6 (2015) 7698.
[21] J. Wang, J. Hao, D. Liu, S. Qin, C. Chen, C. Yang, Y. Liu, T. Yang, Y. Fan, Y. Chen, W. Lei, Nanoscale 9 (2017) 9787-9791.
[22] J. Wang, J. Hao, D. Liu, S. Qin, D. Portehault, Y. Li, Y. Chen, W. Lei, ACS Energy Lett. 2 (2017) 306-312.
[23] L. Ci, L. Song, C. Jin, D. Jariwala, D. Wu, Y. Li, A. Srivastava, Z.F. Wang, K. Storr, L. Balicas, F. Liu, P.M. Ajayan, Nature Mater. 9 (2010) 430.
[24] K. Yuge, Phys. Rev. B 79 (2009) 144109.
[25] R. Geick, C.H. Perry, G. Rupprecht, Phys. Rev. 146 (1966) 543-547.
[26] K. Shirai, S. Emura, S.i. Gonda, Y. Kumashiro, J. Appl. Phys. 78 (1995) 3392-3400.

[27] A.C. Ferrari, S.E. Rodil, J. Robertson, Phys. Rev. B 67 (2003) 155306.
[28] Q. Weng, X. Wang, C. Zhi, Y. Bando, D. Golberg, ACS Nano 7 (2013) 1558-1565.
[29] M. Jalaly, F. José Gotor, M. Semnan, M. Jesús Sayagués, Sci. Rep. 7 (2017) 3453.
[30] C. Kuhrs, Y. Arita, W. Weiss, W. Ranke, R. Schlögl, Top. Catal. 14 (2000) 111-123.
[31] O.L. Krivanek, M.F. Chisholm, V. Nicolosi, T.J. Pennycook, G.J. Corbin, N. Dellby, M.F. Murfitt, C.S. Own, Z.S. Szilagyi, M.P. Oxley, S.T. Pantelides, S.J. Pennycook, Nature 464 (2010) 571.
[32] M.H. Khan, G. Casillas, D.R.G. Mitchell, H.K. Liu, L. Jiang, Z. Huang, Nanoscale 8 (2016) 15926-15933.
[33] H.S.V. Harrach, D. Klenov, B. Freitag, P. Schlossmacher, P.C. Collins, H.L. Fraser, Microsc. Microanal. 16 (2010) 1312-1313.
[34] J.M. Titchmarsh, Ultramicroscopy 28 (1989) 347-351.
[35] K.K. Kim, A. Hsu, X. Jia, S.M. Kim, Y. Shi, M. Dresselhaus, T. Palacios, J. Kong, ACS Nano 6 (2012) 8583-8590.
[36] W.J. Lehmann, C.O. Wilson, J.F. Ditter, I. Shapiro, Infrared Spectrometry in Boron Chemistry, in: BORAX TO BORANES, American Chemical Society, 1961, pp. 139-150.
[37] J.E. Stewart, J. Chem. Phys. 30 (1959) 1259-1265.
[38] J. Coates, Interpretation of Infrared Spectra, A Practical Approach, in: Encyclopedia of Analytical Chemistry, R.A. Meyers, M. L. Mckelvy (Eds.), John Wiley & Sons, Ltd., 2006, pp. 12.
[39] F. Leardini, M.J. Valero-Pedraza, E. Perez-Mayoral, R. Cantelli, M.A. Bañares, J. Phys. Chem. C 118 (2014) 17221-17230.
[40] Z. Huang, T. Autrey, Energy Environ. Sci. 5 (2012) 9257-9268.
[41] S. Sepehri, A. Feaver, W.J. Shaw, C.J. Howard, Q. Zhang, T. Autrey, Cao, J. Phys. Chem. B 111 (2007) 14285-14289.
[42] F. Xiao, S. Naficy, G. Casillas, M. H. Khan, T. Katkus, L. Jiang, H. Liu, H. Li, Z. Huang, Adv. Mater. 27 (2015) 7196-7203.
[43] Y. Zhou, J. Lin, L. Li, X. Pan, X. Sun, X. Wang, J. Catal. 365 (2018) 14-23.
[44] K.H. Lee, H.-J. Shin, B. Kumar, H.S. Kim, J. Lee, R. Bhatia, S.-H. Kim, I.-Y. Lee, H.S. Lee, G.-H. Kim, J.-B. Yoo, J.-Y. Choi, S.-W. Kim, Angew. Chem. Int. Ed. 53 (2014) 11493-11497.
[45] L. Shi, D. Wang, A.-H. Lu, Chin. J. Catal. 39 (2018) 908-913.
[46] J. Diao, Z. Feng, R. Huang, H. Liu, S.B.A. Hamid, D.S. Su, ChemSusChem 9 (2016) 662-666.
[47] W. Qi, W. Liu, B. Zhang, X. Gu, X. Guo, D. Su, Angew. Chem. Int. Ed. 52 (2013) 14224-14228.
[48] P. Giannozzi, S. Baroni, N. Bonini, M. Calandra, R. Car, C. Cavazzoni, D. Ceresoli, G.L. Chiarotti, M. Cococcioni, I. Dabo, A. Dal Corso, S. de Gironcoli, S. Fabris, G. Fratesi, R. Gebauer, U. Gerstmann, C. Gougoussis, A. Kokalj, M. Lazzeri, L. Martin-Samos, N. Marzari, F. Mauri, R. Mazzarello, S. Paolini, A. Pasquarello, L. Paulatto, C. Sbraccia, S. Scandolo, G. Sclauzero, A.P. Seitsonen, A. Smogunov, P. Umari, R.M. Wentzcovitch, J. Phys.: Condens. Matter 21 (2009) 395502.
[49] P. Giannozzi, O. Andreussi, T. Brumme, O. Bunau, M. Buongiorno Nardelli, M.

Calandra, R. Car, C. Cavazzoni, D. Ceresoli, M. Cococcioni, N. Colonna, I. Carnimeo, A. Dal Corso, S. de Gironcoli, P. Delugas, R.A. DiStasio, A. Ferretti, A. Floris, G. Fratesi, G. Fugallo, R. Gebauer, U. Gerstmann, F. Giustino, T. Gorni, J. Jia, M. Kawamura, H.Y. Ko, A. Kokalj, E. Küçükbenli, M. Lazzeri, M. Marsili, N. Marzari, F. Mauri, N.L. Nguyen, H.V. Nguyen, A. Otero-de-la-Roza, L. Paulatto, S. Poncé, D. Rocca, R. Sabatini, B. Santra, M. Schlipf, A.P. Seitsonen, A. Smogunov, I. Timrov, T. Thonhauser, P. Umari, N. Vast, X. Wu, S. Baroni, J. Phys.: Condens. Matter 29 (2017) 465901.
[50] P.E. Blöchl, Phys. Rev. B 50 (1994) 17953-17979.
[51] G. Kresse, D. Joubert, Phys. Rev. B 59 (1999) 1758-1775.
[52] J.P. Perdew, K. Burke, M. Ernzerhof, Phys. Rev. Lett. 77 (1996) 3865-3868.
[53] S.P. Huber, E. Gullikson, R. W.E. Van de Kruijs, F. Bijkerk, D. Prendergast, Phys. Rev. B 92 (2015) 245310.

Graphical Abstract

Description

Carbon-doped boron nitride with uniformly dispersed dopants at nanoscale was obtained. Atomic carbon clusters are removed during oxidative dehydrogenation reaction, leading to the formation of highly active sites for catalytic conversion of ethylbenzene to styrene.